Dynamical Climatology

Parametrization of the upper ocean mixed layer in a tropical ocean GCM.

by

S. Ineson and C. Gordon

DCTN 74

January 1989

Meteorological Office (Met. O. 20)
London Road
Bracknell
Berkshire RG12 2SZ

DYNAMICAL CLIMATOLOGY TECHNICAL NOTE NO. 74

PARAMETRIZATION OF THE UPPER OCEAN MIXED LAYER IN A TROPICAL OCEAN GCM

by

S Ineson and C Gordon

Met O 20 (Dynamical
Climatology Branch)
Meteorological Office
London Road
Bracknell
Berkshire, UK RG12 2SZ

January 1989

NOTE: This paper has not been published. Permission to quote from it should be obtained from the Assistant Director of the above Meteorological Office branch.

1. INTRODUCTION

The sea surface temperature (SST) plays a fundamental role in the complicated interactions between atmosphere and ocean. Its evolution is determined by a number of oceanographic and air - sea interaction processes and in particular by the behaviour of the upper ocean turbulent mixed layer and the flux profiles within this layer. In this note we shall be concerned with the parametrization of the mixed layer in a general circulation model (GCM) of the tropical Pacific ocean (Gordon and Corry, 1989). In the tropical Pacific there is generally a net heating of the ocean surface and the wind stress is lower than in higher latitudes (except directly under the trades). A number of coupled and uncoupled experiments (Gordon and Corry, 1989, Gordon, 1989) have indicated that the modelling of SST is a particularly difficult problem when the wind is low and there is surface heating. In these cases the mixed layer shallows as the surface temperature rises, making the SST sensitive to small changes in surface heat flux. It then becomes particularly difficult to differentiate the problems arising from inadequacies in the forcing functions from those in the mixing parametrization.

It might be thought that in a coupled model the warming of the mixed layer would eventually be balanced by increased evaporation from the surface and the shallowing thereby inhibited. In practice this does not happen because once the SST rises above 27.5 - 28°C convection may occur and the accompanying regions of low level convergence are associated with generally weak winds. This reduction in the wind more than compensates the effects of the increase in SST on the surface evaporation with the result that the evaporation from these warm shallow layers actually decreases. This is discussed in greater detail in Gordon (1989).

A number of models currently use the mixing scheme proposed by Pacanowski and Philander (1981) to parametrize vertical turbulent viscosity and diffusivity. In this scheme the eddy coefficients are functions of a local Richardson number and the functional dependence was determined by tuning GCM simulations of equatorial currents to observed current profiles. The suitability of this scheme to model the processes in the upper mixed layer has not been investigated in any detail.

In the coupled Tropical Ocean Global Atmosphere (TOGA) model simulations performed at the UK Met. Office the ocean model SSTs warm up excessively in the southern central Pacific between 5 - 20°S. This is one of the systematic errors in the model simulations (Gordon, 1989). In order to investigate the cause of this, an uncoupled simulation of the ocean model has been carried out which shows similar errors in the southern central Pacific to those found in the coupled model. In both models the warm water forms in a shallow stable layer. Existing surface heat flux climatologies have large uncertainties in the magnitude of the fluxes, especially in data sparse areas and it is not possible to determine whether the warming occurring in the models is caused by errors in the heat input or by errors in the mixing parametrization. For example, excessive heating, low winds or too little entrainment of colder water by the mixing scheme will all lead to high SSTs. What can be done, however, is to consider the sensitivity of the simulation to changes in the fluxes and to the mixing parameters. This note investigates the sensitivity of the mixed layer simulation in these regions by using a one - dimensional version of the mixing scheme. The mixed layer depths from this version compare well with those from the full 3-dimensional model when the same forcing is used in both.

This note is organized as follows: Section 2 describes the ocean GCM and the results from the uncoupled GCM experiment. Section 3 describes the mixing scheme in detail and Section 4 the one dimensional model developed to test the sensitivity of the scheme to forcing and changes in model parameters. Results of sensitivity experiments are presented in Sections 5 and 6. Section 7 examines the theory behind the mixed layer schemes and finally conclusions are drawn in Section 8.

2. SIMULATION OF THE SEASONAL CYCLE

The ocean model described by Gordon and Corry (1989) (for a summary, see below) has been used to simulate the seasonal changes in the tropical Pacific using the Hellerman and Rosenstein (1983), HR, climatological wind stresses and Esbensen and Kushnir (1981), EK, heat fluxes. Gordon and Corry used a surface heat flux $Q(T)=Q(T_c)+\lambda(T_c-T)$, where $\lambda=-\partial Q/\partial T$, $Q(T_c)$ is the heat flux at the climatological SST, T_c, and T is the surface temperature predicted by the model. The second term in Q(T) allows for the local negative feedback, mainly due to

increasing evaporation, as the SST rises. This formulation is identical to that of Haney (1971) and Haney's effective air temperature, T_{air}^{eff} is obtained by equating Q(T) with $\lambda(T_{air}^{eff}-T)$. Haney forcing prevents the SST from drifting to far from climatology but its use is of limited value in assessing the ocean model response in a fully coupled system, where non local feedbacks can dominate. It is also not desirable to include the feedback term in experiments designed to assess the sensitivity of the simulation to the mixing parametrization since, if this is included, the surface buoyancy flux changes with surface temperature. In the experiment described below the feedback term is not included so that the heat inputs are just the Esbensen and Kushnir (1981) climatological values.

The ocean model is a high resolution version of the Bryan/Cox model (Cox, 1984) covering the tropical Pacific ocean between 30°N and 30°S. The latitudinal resolution is 1 degree at the northern and southern boundaries, reducing smoothly to about 1/3 degree on the equator. The longitudinal resolution is 1½ degrees in the central Pacific, reducing to ½ degree at the coasts (the western boundary is closed in the model). The horizontal eddy viscosity varies with the grid spacing so that in the finer regions of the grid a smaller diffusion coefficient is used which avoids excessive diffusion near the equator and coasts. The lateral eddy diffusivity for temperature and salinity is held constant at a value of 10^7 cm^2s^{-1} throughout the grid. Salinity effects are included in the model but the barotropic part is not included, since tests showed the barotropic current to be typically an order of magnitude less than the near-surface current. The ocean model coastline is less detailed than it might be, given the model resolution. This is because the ocean model used in this study is the same as that used in the coupled GCM studies and the coastline geometry was chosen to match that of the much coarser (2½°×3¾°) resolution atmospheric model. In order to reduce the computer storage required by the model the eastern coastline is distorted south of the equator so that the model coastline lies directly north-south rather than following the South American coast. There are 16 levels in the vertical with a 10m resolution near the surface and a constant depth of 4000m. For the depths of model levels refer to table.1. The K-theory mixing scheme of Pacanowski and Philander (1981) is used to parametrize vertical turbulent mixing. In the upper 20m of the model the coefficient of vertical eddy viscosity has a minimum value of 10 cm^2s^{-1} to compensate for high frequency wind fluctuations following Philander et al (1987). The scheme is described in detail in the next section.

Open boundary conditions in temperature, salinity and momentum are applied at 30°N and 30°S and the effect of these is to keep the longitude-depth profiles of temperature and salinity at the boundaries close to their seasonally varying climatological values as specified by Levitus (1982). The meridional gradient of both current components is set equal to zero at the boundary. In the upper levels this allows (in general) an Ekman drift across the boundaries at 30°N and 30°S. Since the barotropic part is set to zero in the model there is no net mass flux across the boundaries although there can be a net heat flux. These boundary conditions also damp coastal Kelvin waves travelling polewards along the eastern boundary (Gordon, 1985).

The model was integrated using the HR wind stresses and the EK heat fluxes for a period of 5½ months starting from September climatological ocean thermal conditions (Levitus, 1982) and zero currents. Fig.1a shows the climatological SSTs for the period October to February taken from Meteorological Office analyses (Bottomley et al, 1989) and fig.1b the corresponding simulated SSTs. One of the major errors is that 29°C warm water in the central southern Pacific extends too far east as the integration progresses. This warm pool of water is viewed in another way in fig.2 which shows the north-south temperature cross-sections through 135°W for February from the model and from the Levitus climatology. The near surface water between 10-20°S is seen to be 2°C too warm with a highly stratified stable mixed layer near to the ocean surface. A simple explanation of this shallow layer would be excessive surface heating stabilising the upper ocean but an underestimation of the entrainment of cold water from below by the mixing scheme may also be important. In the sections that follow this latter question will be addressed in detail.

It is computationally expensive to perform a large number of sensitivity experiments with the GCM and in some cases it may not be necessary to use the full model. In the central regions of the warm pool in fig.1b the horizontal temperature gradients are small and so local effects can be expected to dominate. Fig.3 shows the vertical temperature profiles for each month through the model integration and also for Levitus for a point at (22°S 125°W). The shallow mixed layer in the model is clearly evident. The purpose of the remainder of this note is to understand this behaviour and assess the sensitivity of the thermal structure to the details of the mixing scheme used and to the specification of the surface forcing.

3. THE MIXING SCHEME

Consider the heat equation in the absence of any internal sources and sinks,

$$\frac{\partial T}{\partial t} + \underline{u}.\underline{\nabla}T + w\frac{\partial T}{\partial z} = 0 \qquad (3.1)$$

where T is temperature, $\underline{u}$ horizontal velocity and w vertical velocity. Taking perturbations about some mean state of equation (3.1) such that $T \Rightarrow T + T'$, $\underline{u} \Rightarrow \underline{u} + \underline{u}'$, and $w \Rightarrow w + w'$, for the remainder of this note unprimed quantities representing the mean and primes indicating perturbations from this, gives

$$\frac{\partial T}{\partial t} + \underline{u}.\nabla T + w\frac{\partial T}{\partial z} + \underline{\nabla}.(\overline{\underline{u}'T'}) + \frac{\partial}{\partial z}(\overline{w'T'}) = 0 \qquad (3.2)$$

where an overbar represents the mean of flux quantities. The scheme used to parametrize the turbulent fluxes, $\overline{\underline{u}'T'}$ and $\overline{w'T'}$, is a first order closure scheme such that

$$\overline{w'T'} = K_H \frac{\partial T}{\partial z} \qquad \overline{\underline{u}'T'} = A_H \underline{\nabla}T \qquad (3.3)$$

where K_H is the coefficient of vertical heat diffusion and A_H the coefficient of horizontal heat diffusion. A similar approach can be applied to close the momentum equation.

The values of vertical eddy viscosity, K_m, and vertical eddy diffusivity, K_H, vary considerably throughout the upper ocean layers. It is, therefore, desirable when simulating the dynamical response of the ocean with a multilevel GCM as described in the previous section to express these coefficients as a function of the mean modelled fields rather than use constant values. There are a number of 'K-theory' mixing schemes (eg. Henderson-Sellers, 1982; Peters et al., 1988). The one used in many tropical GCMs and outlined below is due to Pacanowski and Philander (1981) and is described in detail in that paper.

The strength of turbulent mixing will depend on the stability of the fluid. Following measurements taken in the Atlantic equatorial undercurrent, which suggest, as expected, that mixing processes are dependent to an extent on the shears of the mean currents and following other empirical studies, Pacanowski

and Philander arrive at parametrizations dependent on the Richardson number of the form,

$$K_m = \frac{\nu_o}{(1 + \alpha Ri)^n} + \nu_b \qquad (3.4)$$

$$K_H = \frac{K_m}{(1 + \alpha Ri)} + \kappa_b \qquad (3.5)$$

where ν_o, α and n are adjustable parameters, ν_b and κ_b are background dissipation values and the Richardson number is

$$Ri = \frac{\alpha g \frac{\partial T}{\partial z}}{\left| \frac{\partial \underline{u}}{\partial z} \right|^2} \qquad (3.6)$$

where α is the coefficient of thermal expansion of water and g is gravity.

Pacanowski and Philander considered different regimes for large and small values of the Richardson number and the model response to forcing by eastward wind (such as over the central Indian Ocean in Spring and Autumn) and westward winds (equatorial Pacific). In the latter case the role of net heat flux is important in stabilising the cold upwelling water. Parameters used in the GCM experiment described here were taken to have the following values.

1) Background Parameters

$\nu_b = 0.5 \ cm^2 s^{-1}$

$\kappa_b = 0.05 \ cm^2 s^{-1}$

Pacanowski and Philander used $\nu_b = 1 \ cm^2 s^{-1}$ and $\kappa_b = 0.1 \ cm^2 s^{-1}$ which were the largest values possible under the constraint of minimising the spread of the thermocline over a long integration. ν_b and κ_b used in this experiment lie between these values and those obtained by a fit to data by Peters et al

(1988). There is a lower bound on the model values which is determined by the criteria for numerical stability.

2) Adjustable Parameters

$\nu_o = 55 \text{ cm}^2\text{s}^{-1}$

$n = 2$

$\alpha = 5$

The ocean model response on the equator to eastward winds is an intense eastward equatorial jet. Pacanowski and Philander found that variations in ν_o, the neutral value of the eddy viscosity coefficient, affected both the shear and the speed of the jet, and variations in n and α the speed only. Thus provided the modellers choice in ν_o is sufficiently flexible ($50 \leq \nu_o \leq 100 \text{ cm}^2\text{s}^{-1}$) it is unnecessary for n and α to vary too. Values used for this experiment are those assigned by Pacanowski and Philander. With westward forcing and a net positive heat flux Pacanowski and Philander found their model was relatively insensitive to the size of ν_o provided it was of the order of 50 cm^2s^{-1}

4. THE SINGLE COLUMN MODEL

For reasons of economy it is useful to devise a single column model which will simulate variations in the upper layers of the ocean in response to local forcing and which can be used to investigate the sensitivity of the mixing scheme to imposed forcing and to internal model parameters. This section describes the model used in the sections which follow and examines in what respects results from experiments with this model might be expected to differ from those of the GCM.

Consider a horizontal stress (τ_x, τ_y) acting at the ocean surface, then the linearised equations of motion for a uniformly rotating fluid are

$$\frac{\partial u}{\partial t} - fv = -\frac{1}{\rho}\frac{\partial p}{\partial x} + \frac{1}{\rho}\frac{\partial \tau_x}{\partial z}$$

$$\frac{\partial v}{\partial t} + fu = -\frac{1}{\rho}\frac{\partial p}{\partial y} + \frac{1}{\rho}\frac{\partial \tau_y}{\partial z} \qquad (4.1)$$

where p is pressure, ρ is density, $\underline{u}$ = (u,v) horizontal velocity and f is the Coriolis parameter. The two forces acting on the fluid, namely the horizontal pressure gradient and the vertical gradient of the stress , may be considered separately. The currents produced by the pressure gradient, (u_p,v_p), in the case of steady flow the geostrophic currents, are governed by

$$\frac{\partial u_p}{\partial t} - f v_p = -\frac{1}{\rho}\frac{\partial p}{\partial x} \qquad \frac{\partial v_p}{\partial t} + f u_p = -\frac{1}{\rho}\frac{\partial p}{\partial y} \tag{4.2}$$

The vertical shear of the geostrophic current is related to the horizontal density gradient by the thermal wind equation. In a model with coarse horizontal resolution, so that fine scale density structures are not resolved, most of the current shear will arise from the near surface wind driven currents. (There are exceptions such as in the region above and below the equatorial undercurrent.) The Ekman velocity (u_E,v_E) due to action of the wind stress is confined to a thin friction layer near the ocean surface and described by

$$\frac{\partial u_E}{\partial t} - f v_E = \frac{1}{\rho}\frac{\partial \tau_x}{\partial z} \qquad \frac{\partial v_E}{\partial t} + f u_E = \frac{1}{\rho}\frac{\partial \tau_y}{\partial z} \tag{4.3}$$

It is this Ekman layer that the model presented here aims to simulate.

The single column model uses the first order closure, as illustrated by (3.3), and has the governing equations

$$\begin{aligned}
\frac{\partial u}{\partial t} - fv &= \frac{\partial}{\partial z}\left(K_m\frac{\partial u}{\partial z}\right) - \lambda u \\
\frac{\partial v}{\partial t} + fu &= \frac{\partial}{\partial z}\left(K_m\frac{\partial v}{\partial z}\right) - \lambda v \\
\frac{\partial T}{\partial t} &= \frac{\partial}{\partial z}\left(k_H\frac{\partial T}{\partial z}\right) + \frac{1}{c\rho}\frac{\partial S}{\partial z}
\end{aligned} \tag{4.4}$$

where the subscript 'E' on the velocity components has been dropped, c is the specific heat capacity and S(z) is the penetrative part of the incoming radiative flux. These equations are subject to the boundary conditions

$$\begin{aligned}
K_m\frac{\partial u}{\partial z}\Big|_o &= \frac{\tau_x}{\rho} \qquad K_m\frac{\partial v}{\partial z}\Big|_o = \frac{\tau_y}{\rho} \qquad K_m\frac{\partial u}{\partial z}\Big|_{bottom} = 0 \\
K_H\frac{\partial T}{\partial z}\Big|_o &= \frac{Q}{c\rho} \qquad K_H\frac{\partial T}{\partial z}\Big|_{bottom} = 0
\end{aligned} \tag{4.5}$$

where Q is the heat flux and the terms involving λ provide momentum damping.

The salient features of the GCM are emulated in that the solar radiative penetrative scheme is implemented, the turbulent mixing coefficients are parametrized in the same manner and adjustment of the column takes place at the end of each timestep if the ocean has become convectively unstable due to heat loss. The initial conditions are as those of the GCM model point (22°S,125°W) referred to in Section 2 (ie. in the anomalous warm region) and forcing is by HR wind stresses and EK heat fluxes interpolated for that point.

Forcing by wind stress causes a current to be set up in the uppermost model level. The mixing scheme carries momentum downwards and because of the action of the Coriolis term the current backs with depth. The time independent solution is an Ekman spiral which arises from a balance between the Coriolis and diffusion terms in equations (4.4). When time dependence is included inertial oscillations are also present. Integration of a simple unstratified model by Pollard and Millard (1970) reproduced observed inertial oscillations in mixed layer currents when the model was forced with a time series of measured winds. Their model included a damping term $-\lambda \underline{u}$ which has the effect of introducing a decay timescale for inertial oscillations. Following their work a value of λ of $(4\ \text{day})^{-1}$ has been chosen for the control run.

The time differencing scheme for the Coriolis and damping terms is formulated in semi-implicit form but with parameters such that the integration is essentially explicit. As in the GCM the vertical diffusion calculation is treated explicitly and to avoid a numerical instability arising an iterative procedure is used, effectively reducing the timestep in this part of the model.

To summarise, results from the two models may differ due to advection of heat and momentum into or out of the area although for reasons described in Section 2 these do not dominate the mixed layer response. Pressure gradient and salinity effects are neglected in the column model and a damping term is included in the linearised momentum equations.

5. CONTROL RUN OF THE SINGLE COLUMN MODEL

The single column model was integrated for 5½ months from mid September through to the end of February with monthly climatological data (HR wind stresses and EK heat fluxes) linearly interpolated to three day intervals as forcing for the period. The initial temperature profile was identical to that used in the GCM at (22°S,125°W), a point at which the mixed layer rapidly shallowed as described in Section 2. The results from this experiment are here compared with those from the the GCM simulation and then examined with reference to the forcing data for the period in order to gain insight into the behaviour of the mixing scheme. Variations in the forcing data and in the model parameters will be considered in Section 6.

Isotherms of monthly mean temperature for the duration of the single column integration are shown in fig.4a. Considerable shallowing of the mixed layer occurs from October to December. Thereafter the surface temperature continues to increase but the mixed layer depth decreases only slightly, the intensity of the thermocline increasing. Comparison with the corresponding profiles from the GCM experiment described in Section 2 and Levitus, fig.4b and fig.4c, shows a marked similarity between the single column model and GCM results and the dissimilarity of both to the climatological data. Levitus does indicate a shallowing of the mixed layer but it is not as dramatic as in the model, the climatological mixed layer being deeper and cooler. The GCM mixed layer is warmer than that in the single column model and as the surface forcing for the point is identical in both cases the additional warming in the GCM is due to advection. It can be seen from fig.1b that for most of the period of the model simulation the point is in a region of large horizontal temperature gradients. The surface currents at the point are from the north leading to an advection of warmer water into the region.

Despite the advective effects the similarity in behaviour in the two models indicates that the single column model can provide useful insight into understanding the basic mixed layer response to the surface forcing. In particular, the mixed layer depths are essentially the same in the GCM and single column integration.

Understanding of the reason for the models producing such a shallowing must lie with the model response to the forcing data. During the period the wind stress, fig.5c, shows little variability in magnitude or direction. Initially the net heat flux into the ocean, fig.5b, is negative and for a short period the model convectively adjusts the water column. During this period the mixed layer is deep and Ekman currents reach down to the fifth model level (i.e. 48m) as shown in fig.6a. The mixing coefficients attain their maximum value, that is the neutral plus background value (equations 3.3 and 3.4), because the Richardson number, which is proportional to the vertical temperature gradient, is zero. In January the solar incoming radiation, fig.5a, has attained the southern hemisphere summer maximum. Throughout the intervening period the upper layers of the model are stabilised and the warm shallow layer forms so that from December currents extend only as deep as the second level (i.e. 15m) as shown in fig.6b. Fig.7 illustrates the rapid fall-off of the vertical eddy viscosity coefficients between the upper levels to their background values as the model column becomes stable. During February the net heating is positive but decreasing and the wind stress increasing in magnitude. Note these latter variations cause no effect below the second level in the model.

6. SENSITIVITY TO FORCING AND MODEL PARAMETERS

We now briefly consider the sensitivity of the single column model to the forcing data before discussing the impact of changing the model parameters. The relative importance of the opposing mechanical energy input and buoyancy flux into the model has yet to be established although the stabilising nature of a net heat input on the upper model levels during the control run was noted in the previous Section. In the following paragraphs the sensitivity to the solar flux, which proportionally affects the buoyancy flux, is briefly examined as is the impact of variability of wind stress on short timescales. Tunable model parameters are the momentum damping coefficient, introduced to modify the time dependent solutions of the momentum equations, equations (4.4), and the neutral value of momentum viscosity which indirectly determines the momentum and heat mixing coefficients, equations (3.4) and (3.5) respectively. The effect of varying these parameters is also examined.

6.1 Wind Stress

The reaction of the model, manifested in terms of surface temperature and mixed layer depth, to being forced with multiples of wind stress is shown in fig.8. With increasing wind stress there is an increase in mixed layer depth and a corresponding decrease in surface temperature but it is clear that a large change in forcing is required to appreciably alter the depth of the mixed layer. This is because although an increase in stress will increase the Ekman velocity proportionally, effectively decreasing the Richardson number by the inverse square, the stability of the profile ensures that the Richardson number is significantly greater than one. Hence increases in the downward mixing of heat and momentum are small.

Imposing variability on short timescales to the horizontal component of the wind stress had little impact whether the magnitude of the variability was small or similar to the magnitude of mean wind. Given the reluctance of the mixed layer to deepen with increasing wind stress forcing this is not a surprising result for reasons given above.

6.2 Heat Flux

A decrease in incoming solar radiation of 17 % from November (this is a decrease of less than 40 Wm^{-2}) leads to a mixed layer depth of 40m in February, an increase of 21m from the control. The percentage decrease was chosen so that the net heat flux into the ocean was always positive. Surprisingly the increase in depth was found to be due primarily to the method by which the model treats an unstable profile. Only a given percentage, 75%, of incoming solar radiation is absorbed in the top ocean level, the remainder penetrating to greater depths, and in this experiment the net flux of heat absorbed in the top layer was negative throughout the integration even though the net heat flux balance across the ocean surface was positive from October onwards. By removing heat from the upper level it is possible for the profile to become convectively unstable whereupon the model adjusts the column until a stable profile is attained. In doing so the vertical temperature gradient is eroded, and in this case it became zero between the second and third levels for much of the integration. A vertical temperature gradient of zero implies a Richardson number of zero and maximum values for the mixing coefficients. This

example serves to emphasize the sensitivity to details of the net heat flux into the ocean.

6.3 Momentum damping coefficient

Tests were carried out to determine if the choice of the momentum damping coefficient would affect results, λ being varied from $(0.5\ \text{day})^{-1}$ to $(10\ \text{day})^{-1}$. It was noted that the direction of the current varied slightly and its magnitude increased as expected. Neither of these results had an appreciable effect on mixing and the monthly mean temperatures were the same to within 0.1°C. It was therefore established that the results were largely independent of the choice of λ.

6.4 Neutral value of momentum viscosity

It might be expected that an increase in this parameter would increase the mixing in the model. This was found to be true but to a much lesser extent than anticipated. Certainly the mixing of momentum from the first to the second level increased causing a decrease in surface currents and a decrease in shear between the top levels but because of the nature of the dependence on the Richardson number mixing at depth changed little. The local Richardson number is proportional to the vertical temperature gradient and to the inverse of the square of the current shear. For the duration of the integration the current shear is relatively small and the Richardson number determined predominantly by the temperature gradient. Except for the case in which the ocean column is being convectively adjusted - in this situation the temperature gradient and hence the Richardson number tend to zero - all levels below the very uppermost layers have a local Richardson number which is significantly greater than one. The dependence of the momentum diffusion coefficient on the inverse square of the Richardson number exasperates the problem and mixing tends to background values.

With the neutral value of the momentum mixing coefficient increased to 1000 cm^2s^{-1}, an increase of a factor of 20, the mixed layer depth for the last month of the integration is 20.2m, an increase with respect to the control run of only 1.2m.

7. COMPARISON WITH SIMPLE MIXED LAYER THEORY

Through the period September to February the mixed layer in the southern hemisphere generally shallows as can be seen from both the Levitus dataset and the model data in fig.3. The problem is that the model mixed layer shallows too much leading to excessively high surface temperatures. During such a shallowing phase, Kraus-Turner mixed layer theory predicts the mixed layer depth in a very simple way. This is done by equating the surface input of turbulent kinetic energy with the potential energy changes (work done against buoyancy) in mixing down the surface heat input. When the mixed layer is shallowing the thermal profile beneath the layer is left behind as the mixed layer rises and does not enter the calculation of the new mixed layer depth. This depth is given completely in terms of the surface forcing input and, when penetrative radiative effects are included, is given by the formula

$$h = \frac{2m_o \left(\frac{c}{\alpha g}\right) \frac{\tau^{3/2}}{\rho_w^{1/2}} + \frac{(1-R)\,S_o}{\eta}}{S_o + Q} \qquad (7.1)$$

where m_o is of order unity, ρ_w is the density of water, R=0.67, η is an attenuation coefficient and S_o is the shortwave flux passing through the surface. (The shortwave penetrative flux at a depth z is parametrized by a two band approximation $S(z) = So(Re^{-\eta' z} + (1-R)e^{-\eta z})$, see Paulson and Simpson, 1977, for details). Other symbols are as defined previously. The mixed layer depths calculated from (7.1) with m_o=1 and using the same forcing as used in the single column model gives the mixed layer depth predictions illustrated by the dashed line in figs.4a and 4c. The mixed layer depth calculated from (7.1) is fairly consistent with the Levitus data, fig.4b, but is deeper than the mixed layer predicted by the K-theory scheme, fig.4a.

In order to better understand the difference between the K-theory scheme and the assumptions that give rise to (7.1) it will be useful to consider the turbulent kinetic energy budget in the mixed layer. The turbulent kinetic energy (TKE) equation can be written (Tennekes and Lumley, 1972, p.63)

$$\rho\frac{DE}{Dt} = \alpha\rho_o g\overline{w'T'} - \rho\overline{\underline{u}'w'}\frac{\partial \underline{u}}{\partial z} - \frac{\partial}{\partial z}\overline{\left(w'\left(p' + \frac{1}{2}\rho(\underline{u}'^2+w'^2)\right)\right)} - \varepsilon \qquad (7.2)$$

I II III IV

where standard notation is used. When there is net surface heating term (I) represents the destruction of turbulence by buoyancy and is a sink term, term (II) represents the production of turbulence by the shearing of the mean horizontal current and term (III) is a transport term representing the vertical turbulent transports of pressure fluctuations and TKE. The final term (IV) is a molecular dissipation term and in mixed layer models is usually taken to be linearly proportional to the production terms. In the ocean there are two sources of TKE arising from the mean current shears and also from the surface induced (ie. wavebreaking etc) mixing. Now consider the integration of (7.2) over a column of depth d where d is deep enough so that mixed layer turbulent effects can be ignored and also assume that most of the TKE generated goes into the redistribution of heat (so that ρDE/Dt is small compared to the other terms) then

$$0 = \alpha\rho_o g\int_{-d}^{o}\overline{w'T'}\,dz - \int_{-d}^{o}\rho\overline{\underline{u}'w'}\frac{\partial \underline{u}}{\partial z}dz + \left(-\overline{w'\left(p' + \frac{1}{2}\rho(\underline{u}'^2+w'^2)\right)}\right)\Bigg|_o - \int_{-d}^{o}\varepsilon dz \qquad (7.3)$$

I II III IV

This energy balance equation can be further simplified by assuming the dissipation is linearly related to production and using the scaling

$$\left(-\overline{w'\left(p' + \frac{1}{2}\rho(\underline{u}'^2 + w'^2)\right)}\right)\Bigg|_o - \int_{-\delta}^{o}\rho\overline{\underline{u}'w'}\frac{\partial \underline{u}}{\partial z}\,dz = \rho m_o u_*^3 \qquad (7.4)$$

for the surface boundary condition on the TKE input where u_* is the ocean friction velocity. The contribution from current shears in the wind-wave zone of thickness δ are also included in this term. The models discussed here do not resolve this zone and the effects within it are best treated as a surface flux

of turbulent energy. The quantity (7.4) is often called the windmixing energy. Equation (7.3) then becomes

$$0 = \alpha\rho_o g \int_{-d}^{0} \overline{w'T'}\, dz - m_* \int_{-d}^{-\delta} \rho \overline{u'w'} \frac{\partial u}{\partial z} dz + \rho_o m_o u_*^3 \qquad (7.5)$$

where $m_* < 1$. The first term in (7.5) can also be written in another way. Consider the simple heat equation (ignoring heat advection and penetrative radiation effects although these can easily be included)

$$\frac{\partial T}{\partial t} = \frac{\partial}{\partial z} (-\overline{w'T'}) \qquad (7.6)$$

and multiply by z and integrate over the water column. After integration by parts the result is

$$\frac{\partial P}{\partial t} = \alpha\rho_o g \int_{-d}^{0} \overline{w'T'}\, dz \qquad (7.7)$$

where

$$P = -\alpha\rho_o g \int_{-d}^{0} dz\ zT \qquad (7.8)$$

is the potential energy of the water column. The quantity is physically significant in that the deeper the surface heat input is mixed downwards, the greater the potential energy. Using (7.7) in (7.5) the energy balance can finally be written as

$$\frac{\partial P}{\partial t} = \underbrace{-m_* \int_{-d}^{0} \rho \overline{u'w'} \frac{\partial u}{\partial z} dz}_{\text{I}} + \underbrace{\rho_o m_o u_*^3}_{\text{II}} \qquad (7.9)$$

so that the potential energy can be increased both by mixing arising from current shears and from surface induced effects. The important point regarding (7.8) is that no closure assumptions (ie K-theory or mixed layer hypothesis etc) have been used in deriving it. The difference between the K-theory and simple mixed layer model is apparent explicitly in this equation. The K-theory scheme only contains term (I) and so

$$\frac{\partial P}{\partial t} = m_* \int_{-d}^{0} \rho K_m \left(\frac{\partial u}{\partial z}\right)^2 dz \qquad (7.10)$$

whereas the simple Kraus-Turner mixed layer scheme only has the windmixing term (II) in (7.9) so that

$$\frac{\partial P}{\partial t} = \rho_o m_o u_*^3 \qquad (7.11)$$

so that the energy sources for turbulence are different in each case.

The mixing scheme of Pacanowski and Philander appears to produce insufficient mixing, compared to simple Kraus-Turner mixed layer energy estimates, in a situation in which the mixed layer is rapidly shallowing. The formation of warm shallow layers in the ocean GCM simulation using observed forcing fluxes may, in part therefore, be explained by insufficient entrainment of cold water from below the mixed layer by this K-theory scheme.

8. CONCLUSION

A one dimensional model in which current shears only contain an Ekman component reproduces well the GCM mixed layer depths at a point within the stable region. In such a region it is found that the scheme is relatively insensitive to changes in wind forcing since the shear due to the Ekman currents is comparatively small. As the layers become stabilised the vertical temperature gradient increases in magnitude with the result that the Richardson number becomes large and the mixing tends to background values. Even with large increases, of a factor of four or so, in the stress the profile is so stable that the Richardson numbers remain significantly greater those which would lead to large mixing values. In these highly stable conditions the uncertainties in the magnitudes of surface heat fluxes can play a large part in errors in modelled mixed layer structures and though uncertainties in wind energy are comparatively less important, in general the mixed layer might be expected to deepen as the wind increases.

Kraus-Turner mixed layer theory, based on a simple energy budget, applied to the situation of a shallowing mixed layer indicates that during the shallowing period the input of turbulent kinetic energy is sufficient to result in mixed layer depths comparable with those implied by the Levitus climatological data over much of the period of study and, significantly, to result in depths greater than those predicted by the K-theory scheme. The

sources of turbulent kinetic energy are different in the two schemes, the K-theory scheme deriving energy from the shear of mean currents and the Kraus-Turner scheme from the so called wind mixing energy which is associated with direct turbulent mixing at the ocean surface due to breaking waves, high shears in the wind wave zone, etc.

In conclusion it should be stressed that the scheme of Pacanowski and Philander appears to work reasonably well in mixing momentum and heat in regions of large current shear such as above and below the equatorial undercurrent. However, near the ocean surface the production of turbulent kinetic energy may not be dominated by mean current shears, and the direct input via the wind mixing energy, should not be neglected. The implication for the GCM is that some representation of windmixing effects should be included. This may be achieved either by employing a Kraus-Turner (1967) type model embedded in the GCM or by some simple modification of the K-theory scheme to include windmixing effects. Different methods of doing this, and the effects on the GCM simulation, will be discussed elsewhere.

REFERENCES

Bottomley, M., C. K. Folland, J. Hsiung, R. E. Newel, and D. E. Parker, 1989: *Global Ocean Surface Temperature Atlas (GOSTA).* A joint project of the Meteorological Office and Dept. of Earth, Atmospheric and Planetary Sciences, M.I.T. In press.

Cox, M. D., 1984: A primitive equation, 3-dimensional model of the ocean. GFDL Ocean Group Technical Report No.1.

Esbensen, S. K., and Y. Kushnir, 1981: The heat budget of the global ocean: an atlas based on estimates from surface marine observations. Climate Research Institute, Rep. No. 29, Oregan State University, Corvallis, U.S.A.

Gordon, C., 1985: The development of a coupled GCM suitable for modelling studies in TOGA. In proceedings of Workshop on comparison of simulations by numerical models of the sensitivity of the atmospheric circulation to SST anomalies, NCAR, Boulder.

Gordon, C., 1989: Tropical ocean-atmosphere interactions in a coupled model. To appear in Phil. Transaction of the Royal Society, Special Issue on the 'Dynamics of the Coupled Atmosphere and Ocean'.

Gordon, C., and R. A. Corry, 1989: A model simulation of the seasonal cycle in the tropical Pacific ocean using climatological and modelled forcing. (In preparation).

Haney, R. L., 1971: Surface thermal boundary condition for ocean circulation models. *J. Phys. Oceanogr.*, **1**, 241-248.

Hellerman, S., and M. Rosenstein, 1983: Normal monthly windstress over the world ocean with error estimates. *J. Phys. Oceanogr.*, **13**, 153-168.

Henderson-Sellers, B., 1982: A simple formula for vertical eddy diffusion coefficients under constraints of non-neutral stability. *J. Geophys. Res.*, **87**, 5860-5864.

Kraus, E. B., and J. S. Turner, 1967: A one dimensional model of the seasonal thermocline: II, The general theory and its consequences. *Tellus*, **19**, 98-106.

Levitus, S., 1982: *Climatological Atlas of the World Ocean*. NOAA Prof. Paper 13, U.S. Govt. Printing Office, Washington. D.C.

Pacanowski, R. C., and S. G. H. Philander, 1981: Parameterization of vertical mixing in numerical models of tropical oceans. *J. Phys. Oceanogr.*, **11**, 1443-1451.

Paulson, C. A. and J. J. Simpson, 1977: Irradiance measurements in the upper ocean. *J. Phys. Oceanogr.*, **7**, 952-956.

Peters, H., M. C. Gregg, and J. M. Toole, 1988: On the parameterization of equatorial turbulence. *J. Geophys. Res.*, **93**, 1199-1218.

Philander, S. G. H., W. J. Hurlin, and A. D. Seigel, 1987: Simulation of the seasonal cycle of the tropical Pacific ocean. *J. Phys. Oceanogr.*, **17**, 1986-2002.

Pollard, R. T., and Millard, R. C., 1970: Comparison between observed and simulated wind-generated inertial oscillations. *Deep-Sea Res.*, **17**, 813-821

Tennekes, H., and J. L. Lumley, 1972: *A first course in turbulence*. M.I.T. Press, Cambridge, Massachusetts.

LEVEL	DEPTH
1	5m
2	15m
3	25m
4	35m
5	48m
6	67m
7	96m
8	139m
9	204m
10	301m
11	447m
12	666m
13	996m
14	1490m
15	2232m
16	3339m

Table.1. Depth of mid-point of vertical ocean levels.

Fig.1a. Sequence of climatological sea surface temperatures taken from Meteorological office analyses for the equatorial Pacific Ocean, October to February.

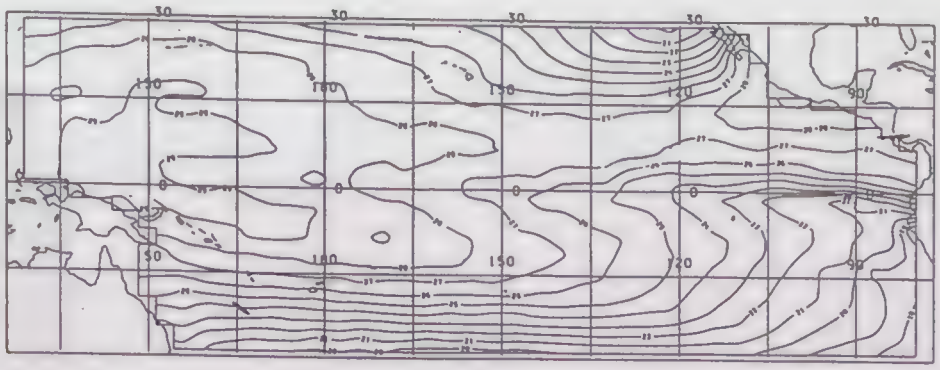

Fig.1a. October. Climatology

Fig.1b. Sequence of equatorial Pacific Ocean Model sea surface temperatures, October to February. Comparison with fig.1a illustrates the gradual departure of model SSTs from climatology. By February excessively high model SSTs are prevalent in the west and central South Pacific.

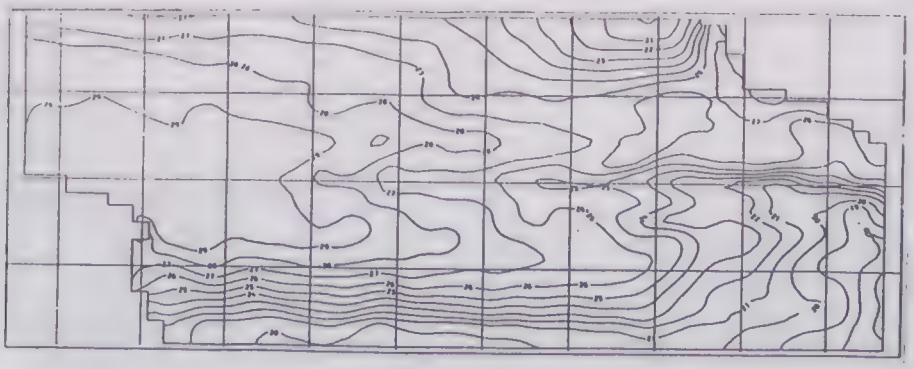

Fig.1b. October. Model

continued overleaf...

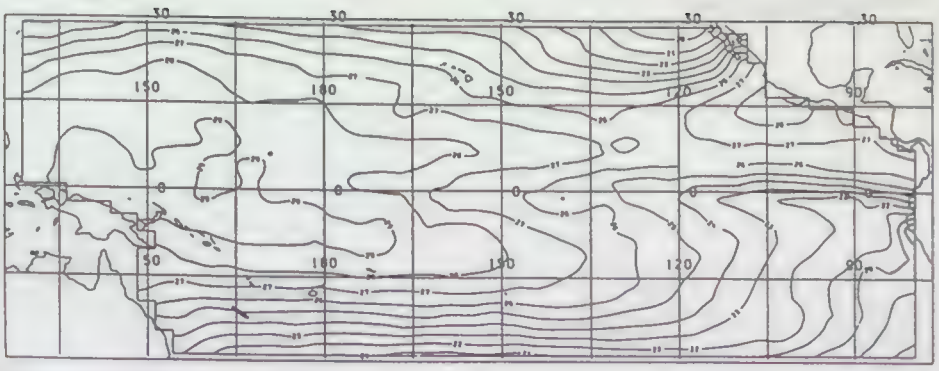

Fig.1a. November. Climatology

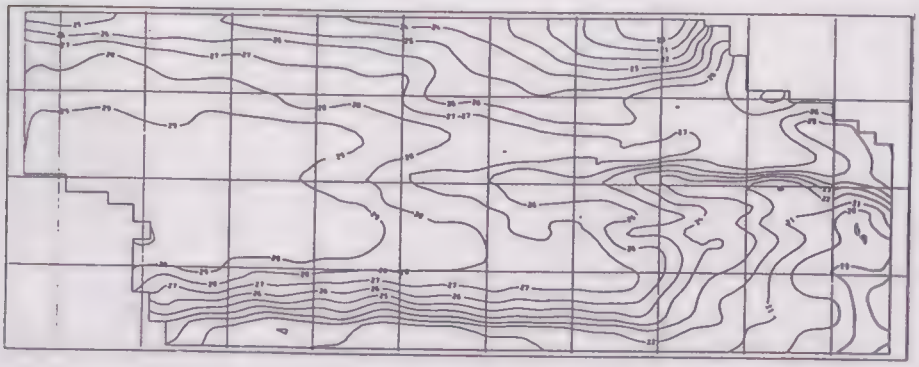

Fig.1b. November. Model

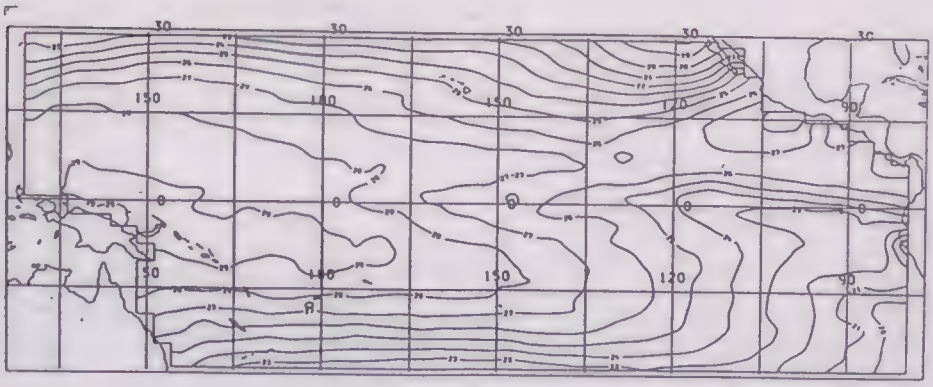

Fig.1a. December. Climatology

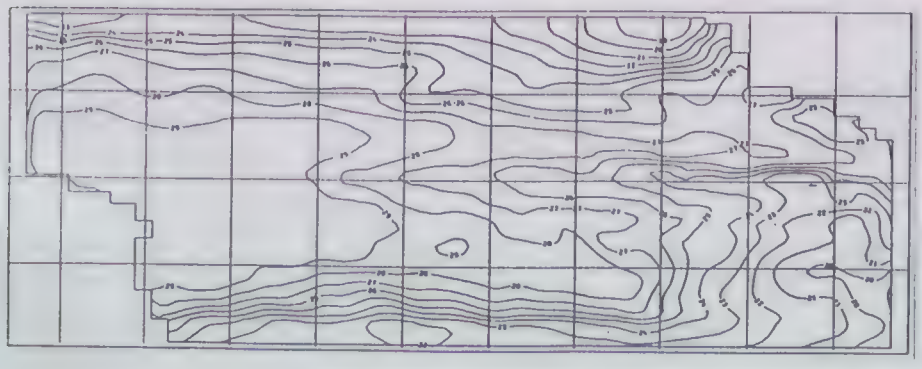

Fig.1b. December. Model

continued overleaf...

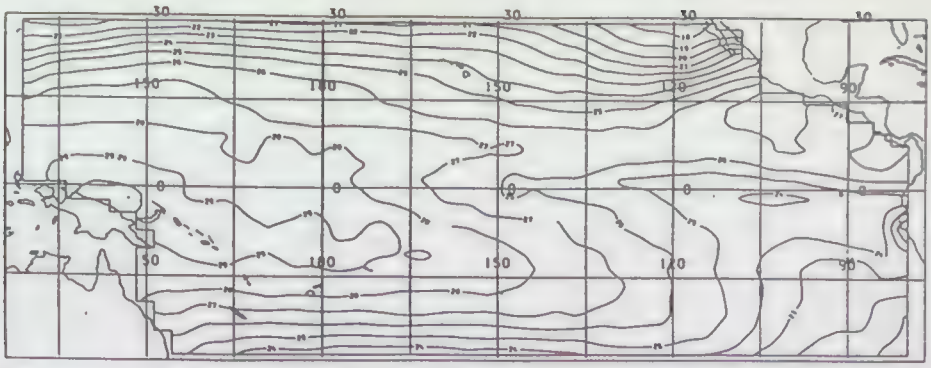

Fig.1a. January. Climatology.

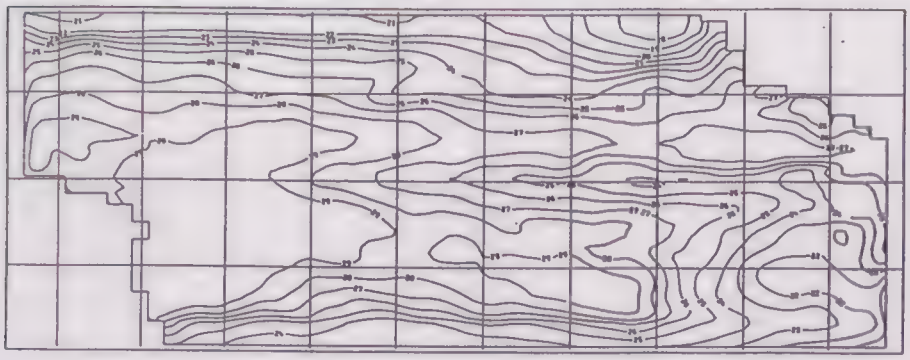

Fig.1b. January. Model.

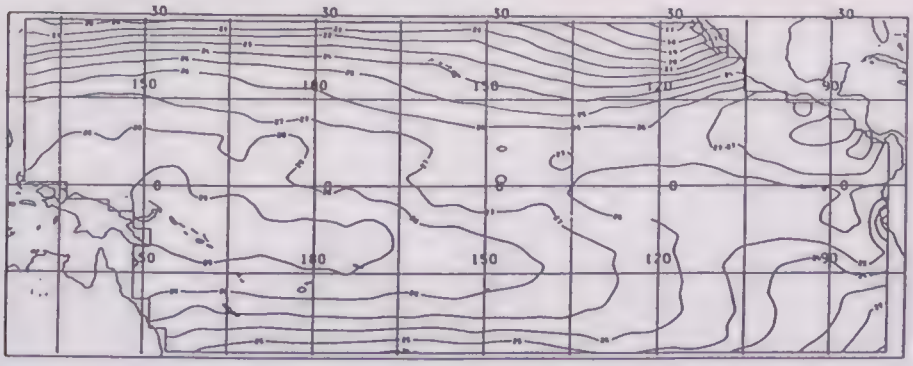

Fig.1a. February. Climatology.

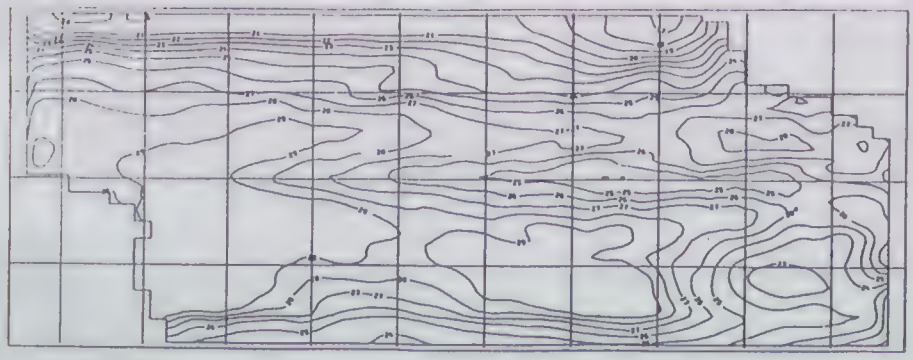

Fig.1b. February. Model.

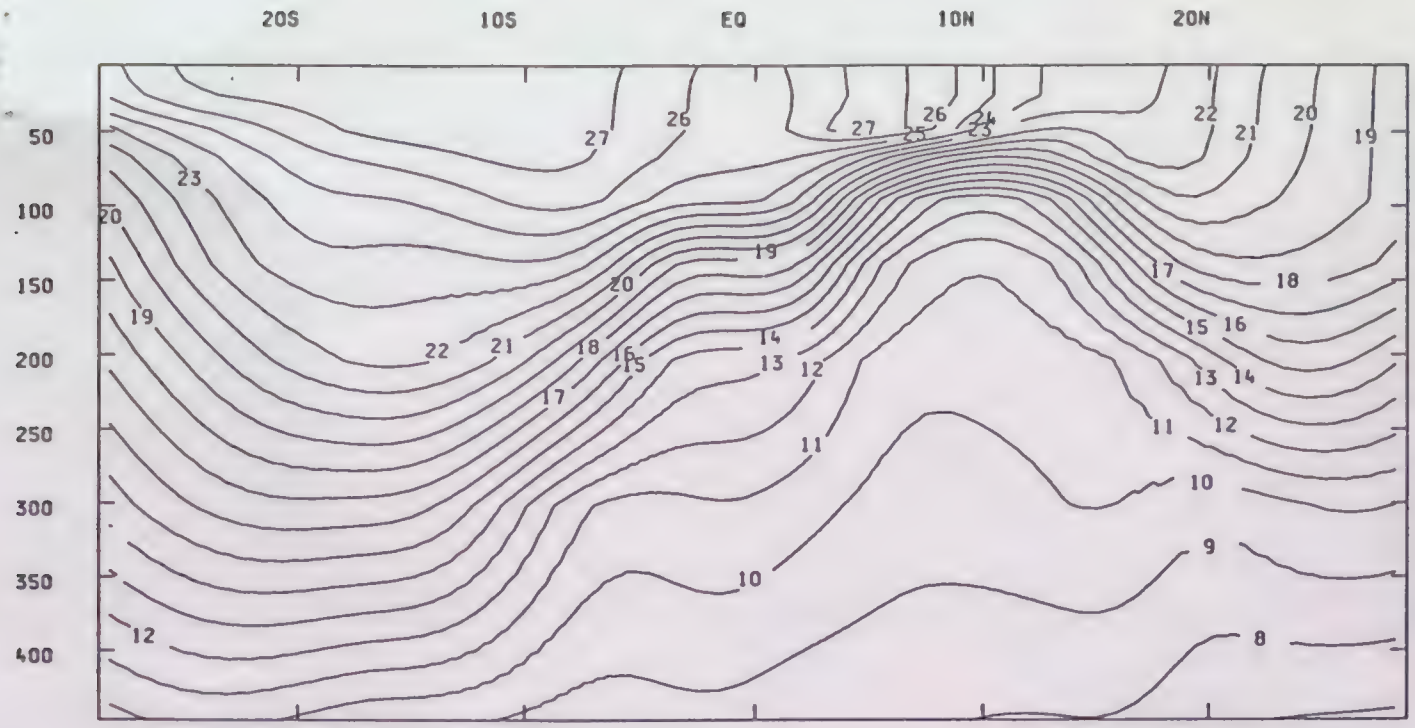

Fig.2a. Climatological (Levitus) meridional cross section of temperature for the equatorial Pacific taken through 135°W for February.

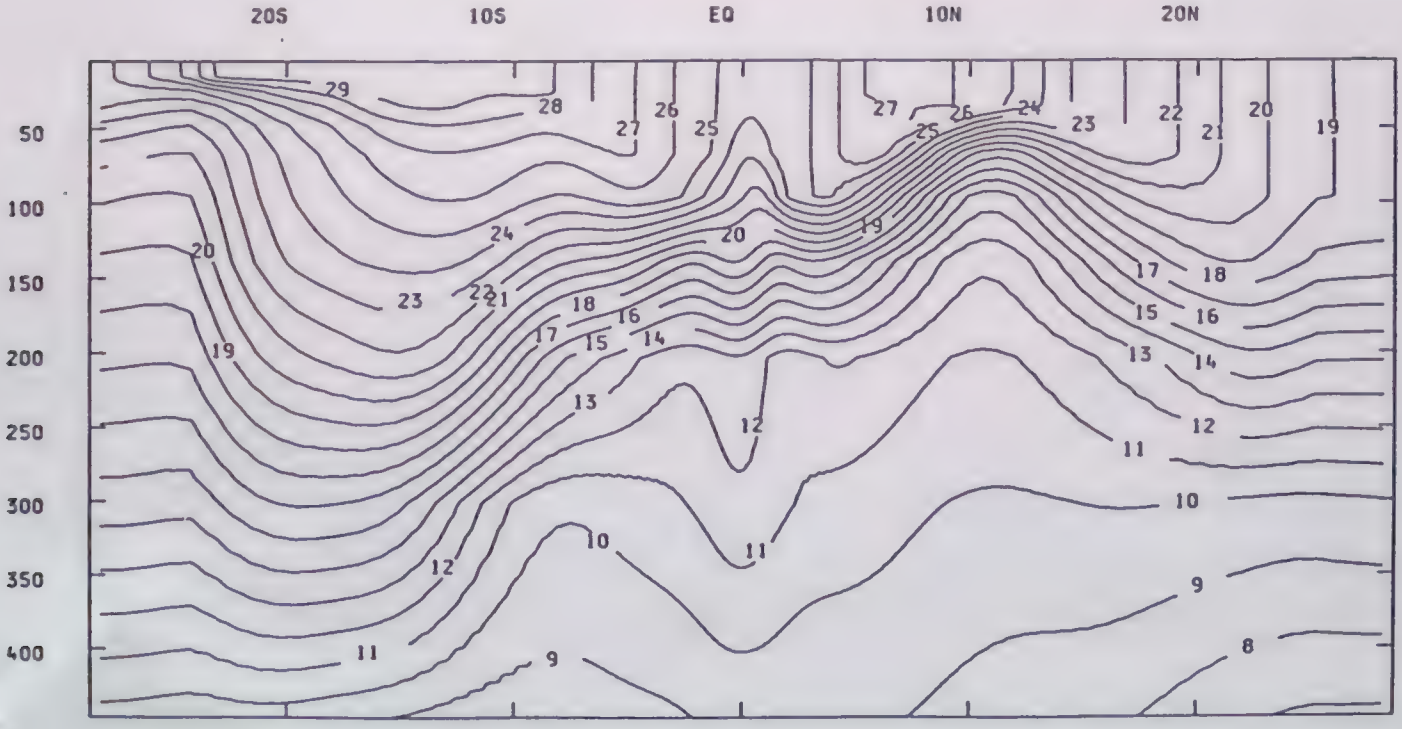

Fig.2b. As in fig.2a but model temperatures. Note the general similarity between model and climatology except for the region 5°S-25°S where a shallowing of the mixed layer depth is accompanied by anomalously high SSTs.

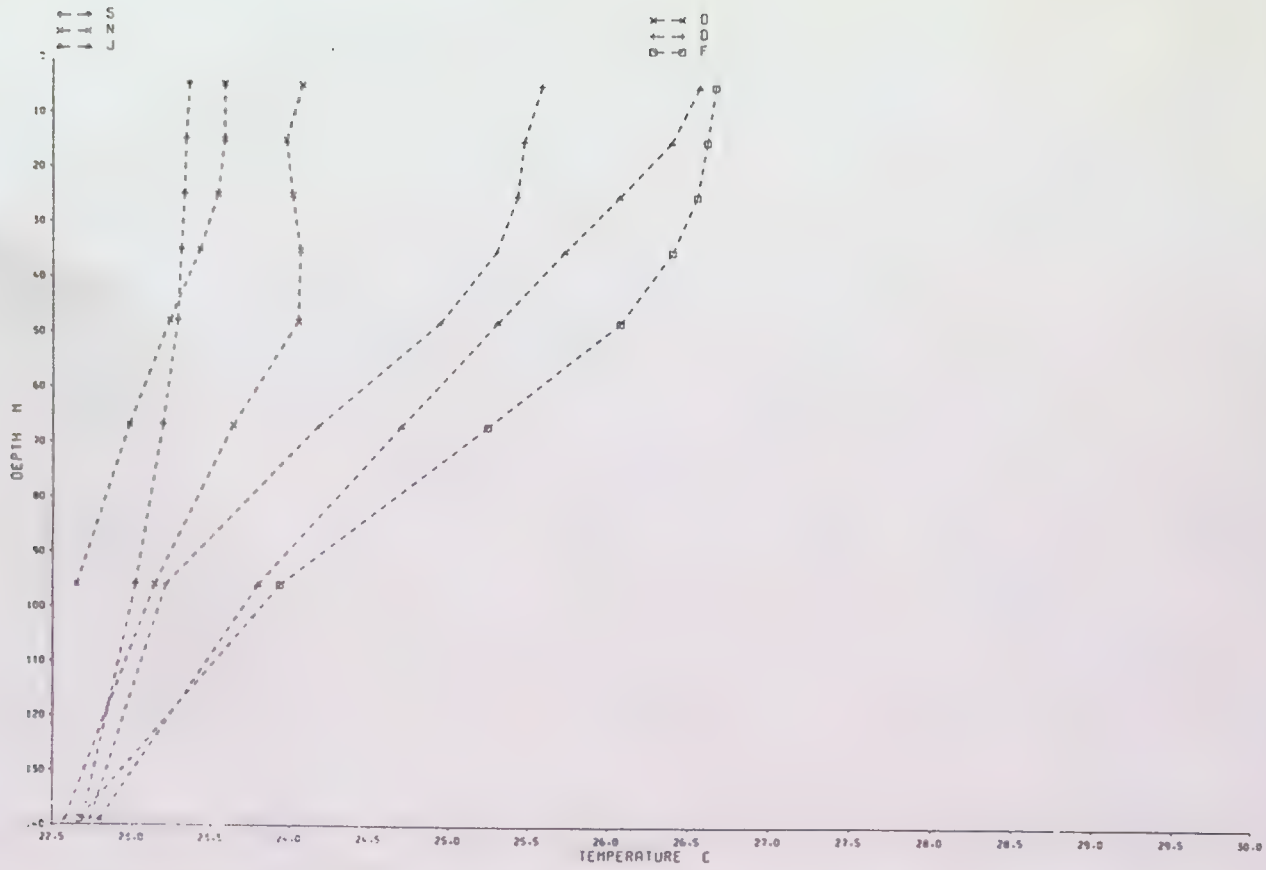

Fig.3a. Climatological (Levitus) temperature profile for months September to February at (22°S,125°W).

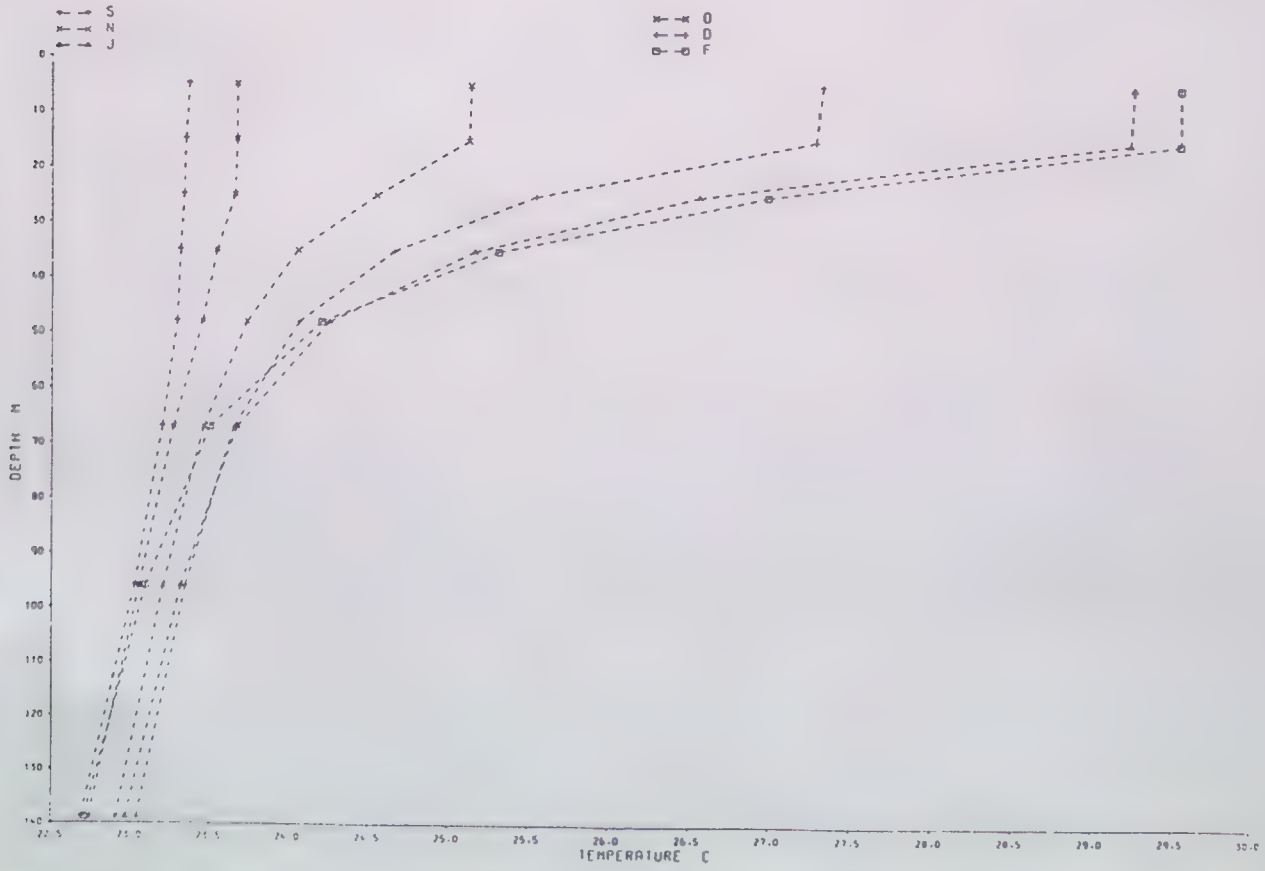

Fig.3b. As in fig.3a but model temperatures. Comparison with fig.3a illustrates the high model SSTs associated with rapid shallowing of the model mixed layer.

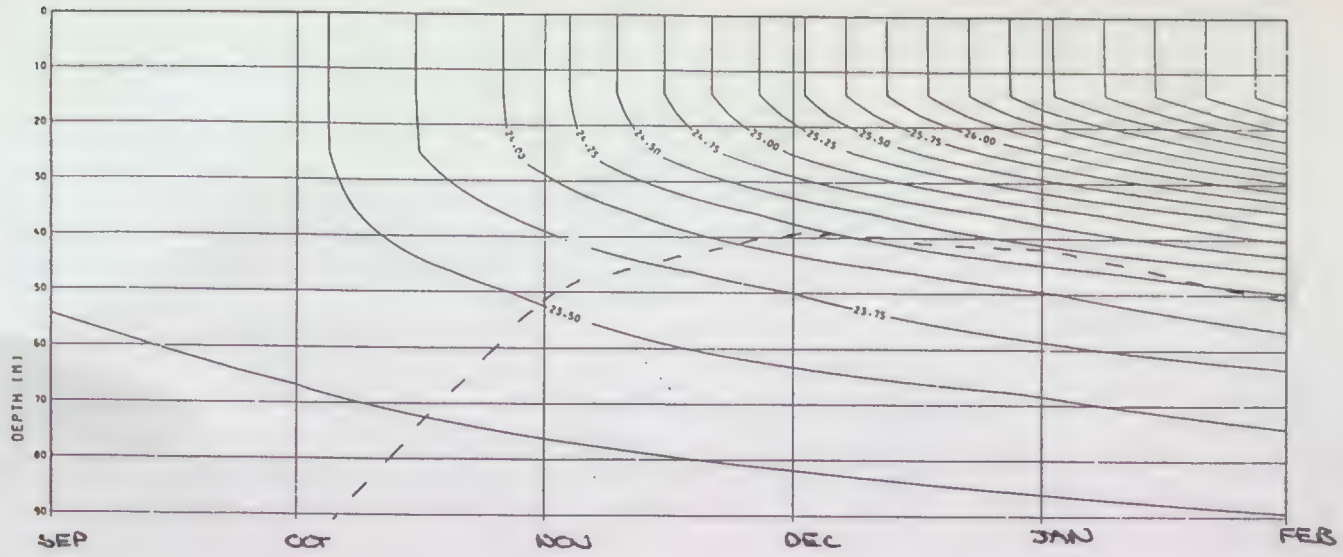

Fig.4a. Isotherms of single column model temperature, (22°S,125°W), for September to February. The dashed line indicates the theoretical mixed layer depth calculated by considering the energy balance between bouyancy forces and turbulent kinetic energy derived from surface wind mixing energy.

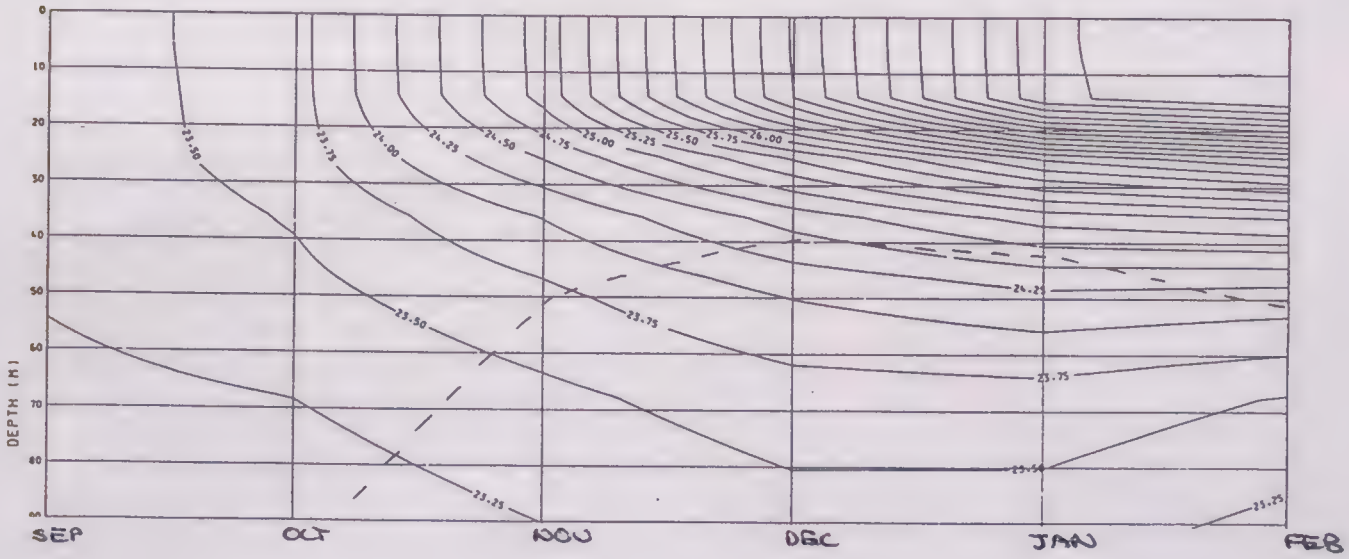

Fig.4b. As in fig.4a but for the 3-dimensional GCM model temperatures.

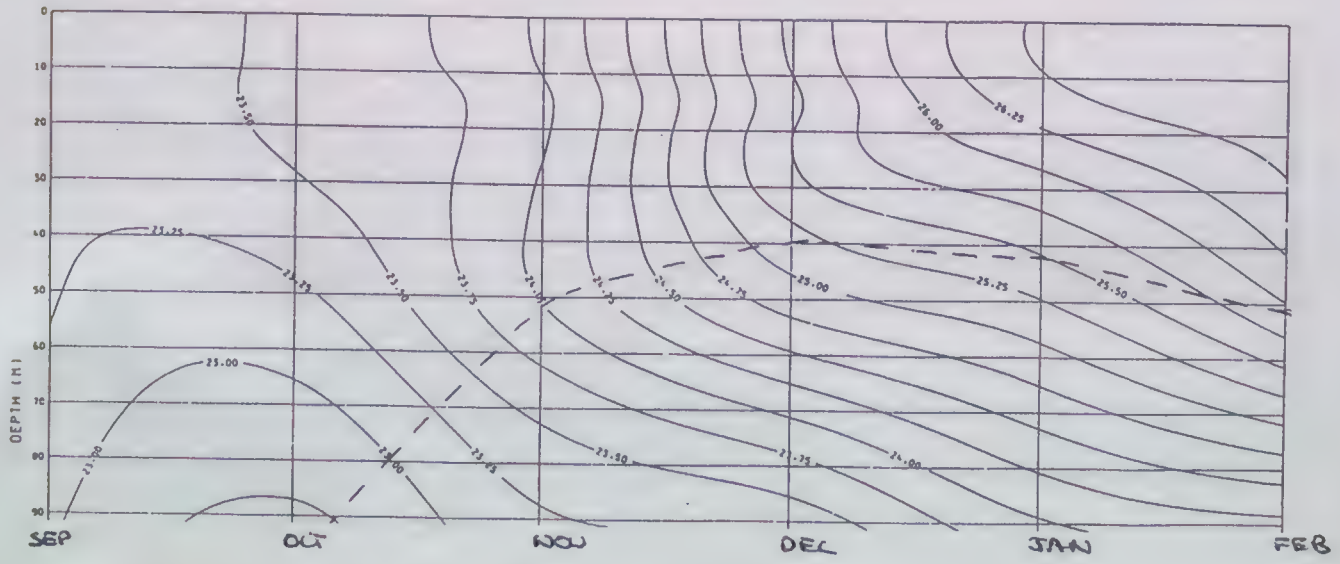

Fig.4c. As in fig.4a but for climatology (Levitus).

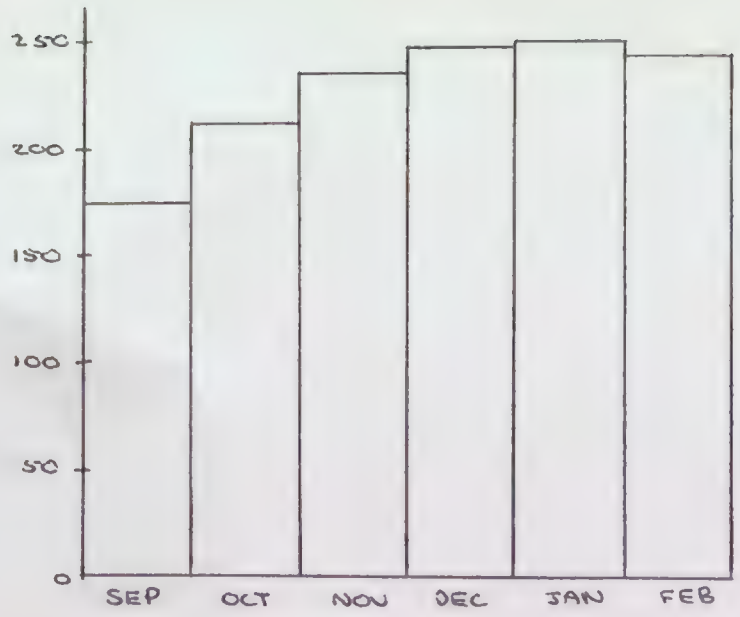

Fig.5a. Forcing data for single column model integration at (22°S,125°W): Incoming solar radiation (Wm^{-2}).

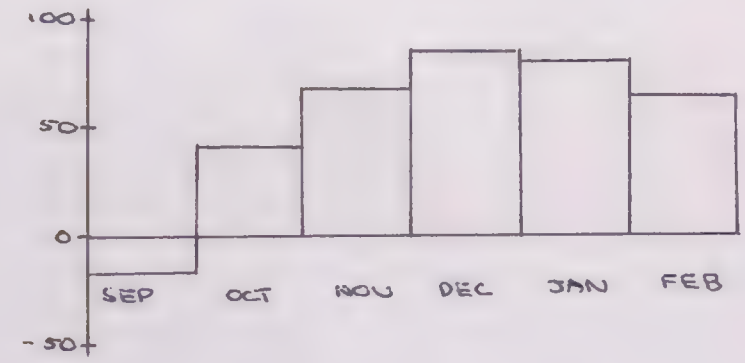

Fig.5b. As in fig.5a: Net downward heat flux (Wm^{-2}). Except during September there is a net input of heat into the ocean at this point.

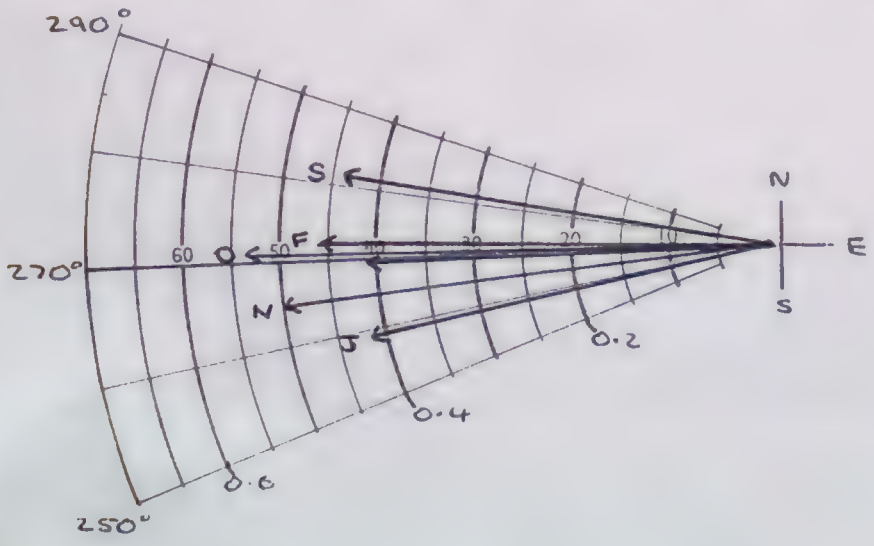

Fig.5c. As in fig.5a: Wind Stress (dyne/cm^2). As the wind remains relatively constant through the period and there is a net heat input, the ocean mixed layer will shallow as already seen in the climatological data.

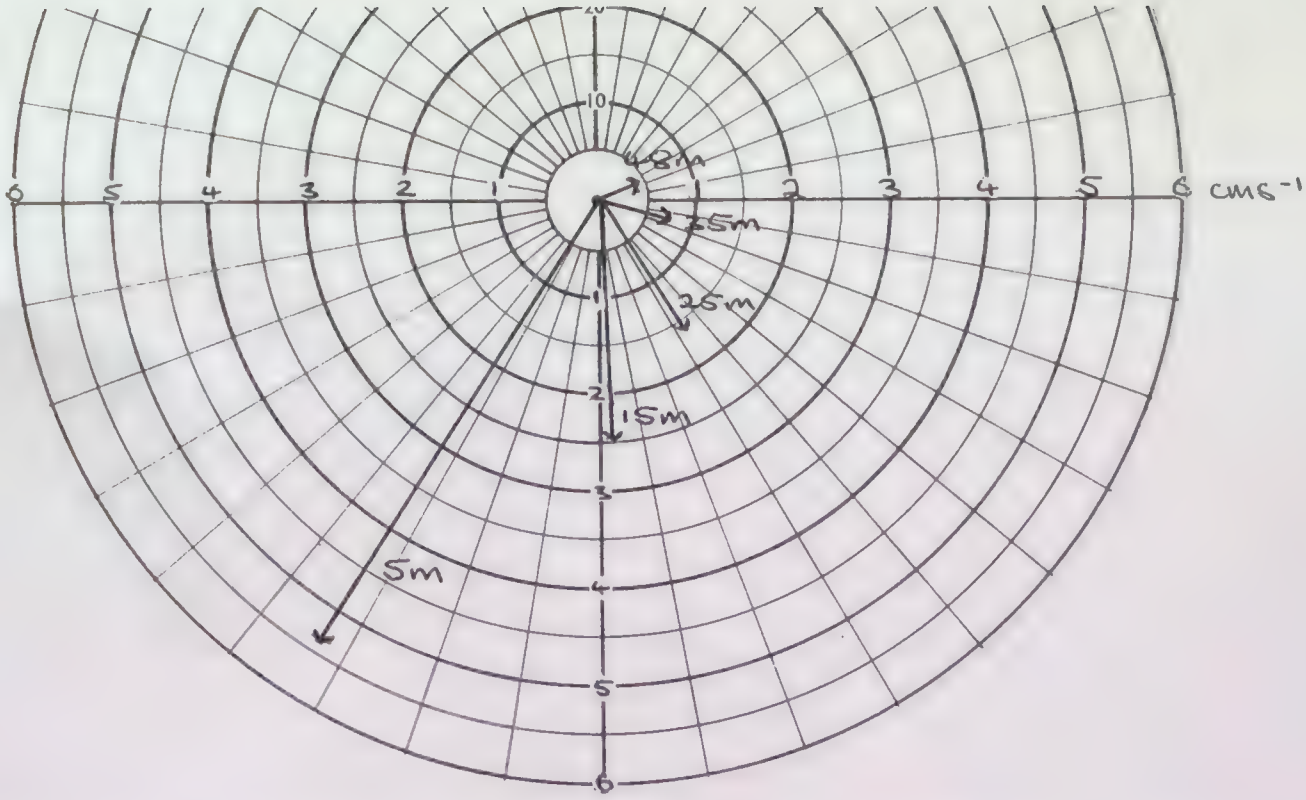

Fig.6a. Single column model Ekman currents for a timestep early in the integration. Convective adjustment has lead to the upper ocean becoming neutrally stable and the Ekman layer penetrates deep down the column.

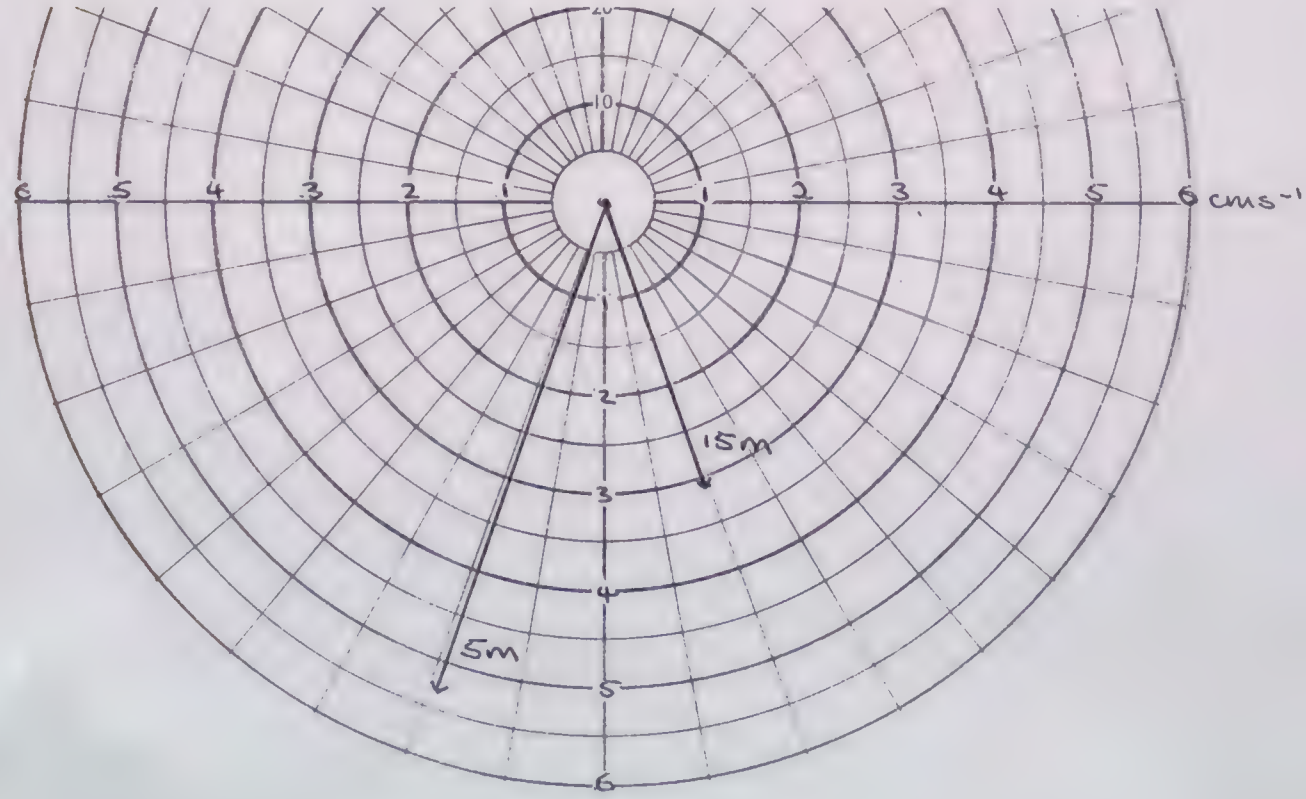

Fig.6b. As for fig.6a but for a timestep towards the end of the integration. The net heat input has stabilised the ocean column resulting in a thin Ekman layer.

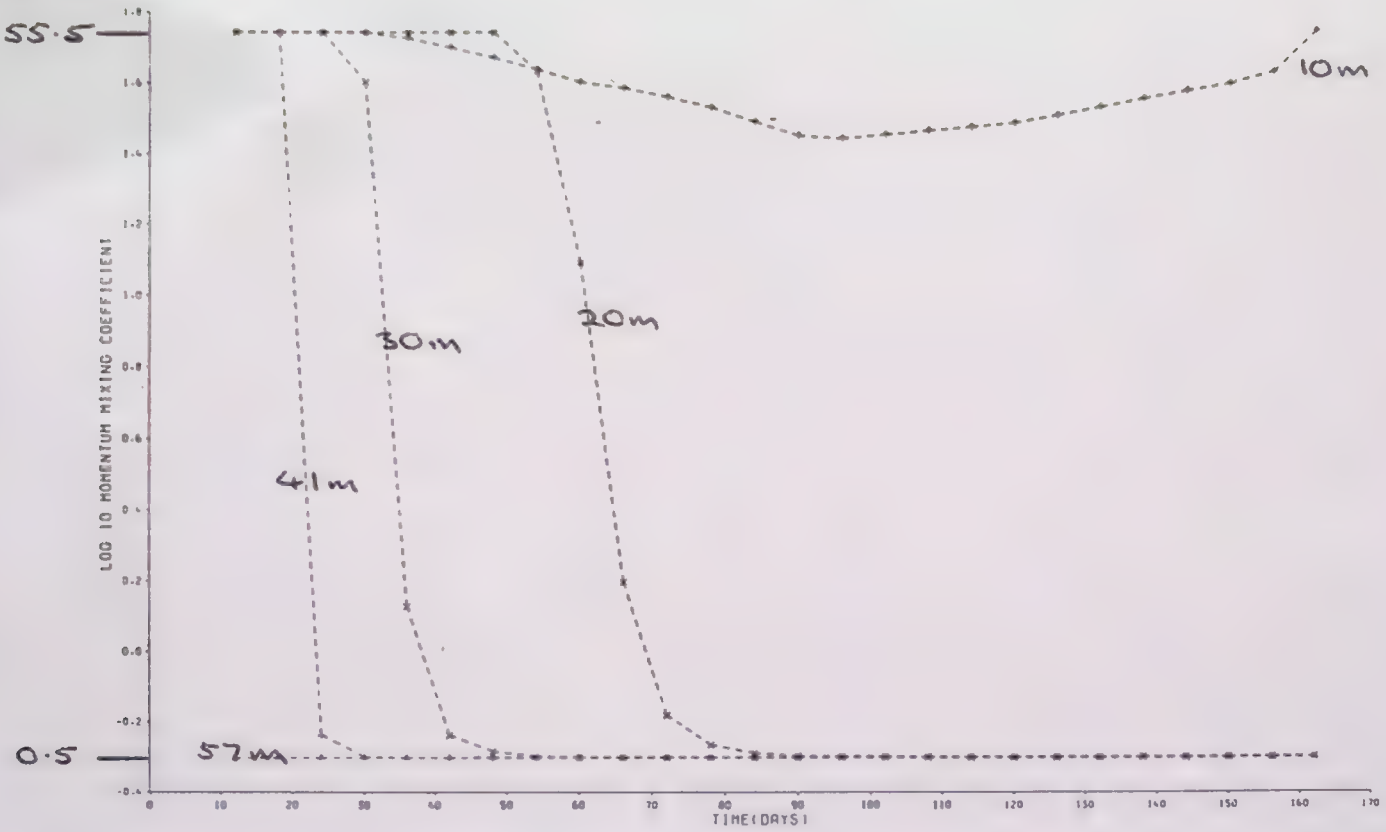

Fig.7. Coefficient of momentum viscosity between six levels for the duration of the single column model integration. If the column is neutrally stable the mixing coefficient attains its maximum value. As the integration progresses heating of the column creates a vertical temperature gradient and mixing coefficients rapidly fall off to background values since small current shears mean that the Richardson number becomes appreciably greater than one.

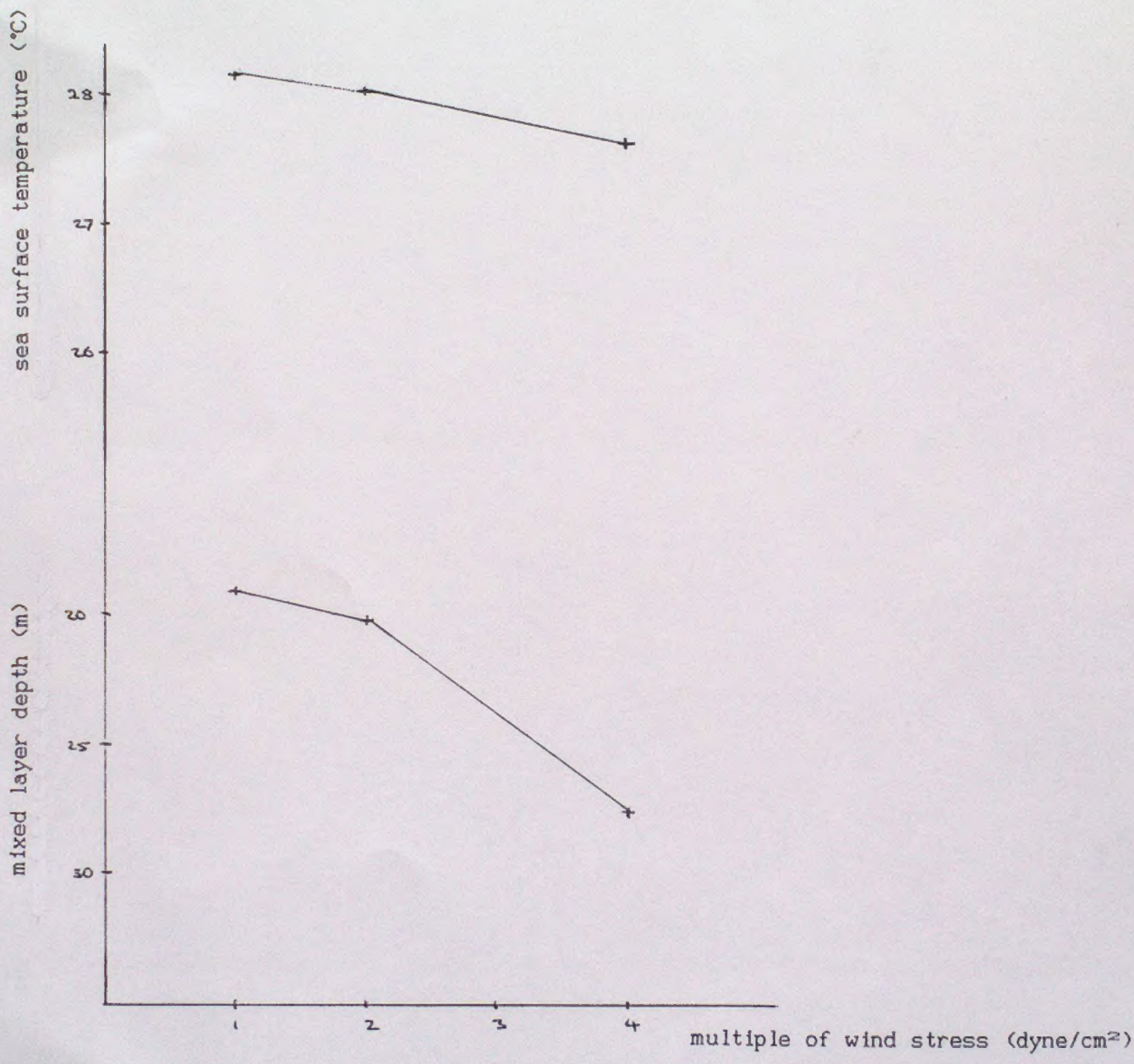

Fig.8. Single column model sea surface temperature and mixed layer depth at (22°S,125°W) for February plotted as a function of wind stress. These results illustrate the apparent insensitivity of the mixing scheme to fluctuations in wind stress in this type of stable ocean regime.

DYNAMICAL CLIMATOLOGY TECHNICAL NOTES

DCTN 1	June 1984	A scheme for incorporating the thermodynamic sea-ice model into a coupled ocean-atmosphere model. C Gordon and M Bottomley
DCTN 2	Sept 1984	The parametrization of the upper ocean mixed layer in coupled ocean/atmosphere models. C Gordon and M Bottomley
DCTN 3	Sept 1984	The response of a simple thermodynamic sea-ice model to GCM forcing appropriate for perennial sea-ice. M Bottomley
DCTN 4	Sept 1984	Potential vorticity in the stratosphere derived using data from satellites. S A Clough, N S Grahame and A O'Neill
DCTN 5	Sept 1984	Simulation of the seasonal cycle of SST using globally specified climatological data to force simple ocean models. N S Grahame
DCTN 6	Sept 1984	Development of an improved GCM radiation scheme. A Slingo and R C Wilderspin
DCTN 7	Sept 1984	On the specification of surface fluxes in coupled atmosphere/ocean general circulation models. J F B Mitchell, C A Wilson and C M Price
DCTN 8	Sept 1984	A survey of possible repercussions of the Soviet river reversal programme on Arctic sea-ice. H Cattle
DCTN 9	Oct 1984	A study of a strong stratospheric warming during January 1982 T D A Fairlie
DCTN 10	Nov 1984	An intercomparison of the Met O 11 N45 model and the Met O 20 11-level model on the Cyber 205 J F Dyson
DCTN 11	Nov 1984	Simulation of observed time series of temperature and precipitation over eastern England. D N Reed
DCTN 12	Nov 1984	Forecasts and analyses of the onset of the Southwest monsoon. R Kershaw
DCTN 13	Nov 1984	On modelling the effects of CO_2 on climate. J F B Mitchell
DCTN 14	Dec 1984	Development of a revised longwave radiation scheme for an atmospheric general circulation model. A Slingo and R C Wilderspin
DCTN 15	Jan 1985	Rossby wavetrains in the stratosphere forced by localised disturbances in the troposphere. C J Marks (Oxford), A O'Neill and V D Pope

DYNAMICAL CLIMATOLOGY TECHNICAL NOTES

DCTN 16	Jan 1985	Observing system experiments using the Meteorological Office's 15-level model. R A Bromley
DCTN 17	Feb 1985	Atmospheric general circulation simulation of the climate of the Mediterranean region. H Cattle
DCTN 18	Feb 1985	Diurnal variation and cloud in a general circulation model. C A Wilson and J F B Mitchell
DCTN 19	Feb 1985	The sensitivity of the Saharan region in a general circulation model. W M Cunnington and P R Rowntree
DCTN 20	Mar 1985	The impact of aircraft observations on analyses and forecasts from the operational 15-level model. B R Barwell
DCTN 21	Mar 1985	Non-linear effects on heat-induced circulation of the tropical atmosphere. A E Gill and P J Phlips
DCTN 22	Apr 1985	Simulation of cloudiness with the U.K. Meteorological Office 11-layer AGCM. A Slingo and R C Wilderspin
DCTN 23	Apr 1985	An integrated approach to the representation of cloud processes. R N B Smith
DCTN 24	May 1985	Nuclear Winter: Calculations of the shortwave radiative effects of soot aerosols. A Slingo and P Goldsmith
DCTN 25	Jul 1985	Sea ice and the Antarctic winter circulation: a numerical experiment. J F B Mitchell and T S Hills
DCTN 26	Jul 1985	A Budyko-Sellers model for study of ocean-atmosphere interaction. W J Ingram
DCTN 27	Aug 1985	The effect of a shoaling thermocline on equatorially-trapped Kelvin waves. A E Gill and B A King
DCTN 28	Sept 1985	CO_2 climate sensitivity and model dependence of results. J F B Mitchell, C A Wilson and W M Cunnington
DCTN 29	Sept 1985	Handbook of the Meteorological Office 11-layer atmospheric general circulation model. Volume 1 : Model Description Edited by A Slingo
DCTN 30	Sept 1985	Impact of land surface variations on African rainfall in general circualation models. P R Rowntree, M F Wilson and A B Sangster

DYNAMICAL CLIMATOLOGY TECHNICAL NOTES

DCTN 31 Nov 1985 The annual cycle of sea level in the eastern tropical Pacific.
G R Bigg and A E Gill

DCTN 32 Nov 1985 An analytic model of the heat-induced tropical circulation in the presence of a mean wind.
P J Phlips and A E Gill

DCTN 33 Nov 1985 The effect of resolution and diffusion on the simulated climate.
J F Dyson

DCTN 34 Jan 1986 Rossby adjustment over a step.
M K Davey, A E Gill, E R Johnson and P F Linden

DCTN 35 Jan 1986 Issues concerning the evaluation of effective surface roughness of heterogeneous terrain.
D J Carson

DCTN 36 Mar 1986 Climate sensitivity and past climates : evidence from numerical studies
J F B Mitchell

DCTN 37 Mar 1986 Parametrizations of land-surface processes in Meteorological Office numerical weather prediction and climate models
D J Carson

DCTN 38 Apr 1986 Modelling of land-surface processes and their influence on European Climate
D A Warrilow, A B Sangster and A Slingo

DCTN 39 Apr 1986 Simulation of climatic change due to increased CO_2
J F B Mitchell

DCTN 40 May 1986 On the interpretation of the Eliassen-Palm flux divergence.
Part I : Theory
D G Andrews

DCTN 41 June 1986 Experiments on tropical circulation with a simple moist model.
M K Davey and A E Gill

DCTN 42 Jun 1986 Parameter regimes for studying isolated eddies.
P D Killworth and M K Davey

DCTN 43 Jun 1986 A comparison of the impact of an envelope orography and of a parametrization of orographic gravity-wave drag on model simulations.
A Slingo and D W Pearson

DCTN 44 Jul 1986 The effect of a sea-surface temperature anomaly on a prediction of the onset of the south-west monsoon over India.
R Kershaw

DCTN 45 Jul 1986 An introduction to the parametrization of land-surface processes.
D J Carson

DYNAMICAL CLIMATOLOGY TECHNICAL NOTES

DCTN 46 Sept 1986 Lateral boundaries and the heat-induced flow in the tropical atmosphere.
P J Phlips and A E Gill

DCTN 47 Nov 1986 Simulation of the diurnal cycle of outgoing longwave radiation with an atmospheric GCM.
A Slingo, R C Wilderspin and S J Brentnall

DCTN 48 Feb 1987 A 2 x CO_2 climate sensitivity experiment with a global climate model including a simple ocean
C A Wilson and J F B Mitchell

DCTN 49 Feb 1987 Sensitivity of the Met O 20 11-layer model to increased land surface roughness length
C C Heasman

DCTN 50 Feb 1987 The influence of atmospheric waves on the general circulation of the middle atmosphere
D G Andrews

DCTN 51 Feb 1987 Transport mechanisms in the middle atmosphere: an introductory survey
D G Andrews

DCTN 52 Mar 1987 The Met O 20 stratosphere-mesosphere model
M Fisher

DCTN 53 Apr 1987 Simulations of linear and nonlinear disturbances in the stratosphere
A O'Neill and V D Pope

DCTN 54 Apr 1987 Aspects of dynamics of the middle atmosphere inferred using data from a satellite and from a numerical model
T D A Fairlie and A O'Neill

DCTN 55 Apr 1987 The seasonal evolution of the stratosphere in the northern hemisphere
A O'Neill and V D Pope

DCTN 56 Apr 1987 The adjustment of numerical weather prediction models to local perturbations
B R Barwell and R A Bromley

DCTN 57 Jun 1987 Climate simulations for 9000 years before present: Seasonal variations and the effect of the Laurentide ice sheet
J F B Mitchell, N S Grahame and K J Needham

DCTN 58 Aug 1987 Climatic effects of nuclear war: the role of atmospheric stability and ground heat fluxes.
J F B Mitchell and A Slingo

DCTN 59 Oct 1987 The stratospheric major warming of winter 1984/85: observations and dynamical inferences.
T D A Fairlie and A O'Neill

DCTN 60 Oct 1987 Some comparisons between the middle atmosphere dynamics of the southern and northern hemispheres
D G Andrews

DYNAMICAL CLIMATOLOGY TECHNICAL NOTES

DCTN 61	Jan 1988	Early winter in the northern stratosphere. M N Juckes and A O'Neill
DCTN 62	Feb 1988	Single column model tests of the Rowntree convection scheme using GATE data. D Gregory
DCTN 63	Mar 1988	The antarctic winter; simulations with climatological and reduced sea-ice extents. J F B Mitchell and C A Senior
DCTN 64	Mar 1988	An investigation of the Gates asynchronous coupling strategy using a simple energy-balance model. D L Roberts
DCTN 65	Apr 1988	The effect of improved physical parametrizations on simulations of cloudiness and the earth's radiation budget. A Slingo, R C Wilderspin and R N B Smith
DCTN 66	May 1988	Comparison of data and derived quantities for the middle atmosphere of the southern hemisphere. W L Grose and A O'Neill
DCTN 67	Aug 1988	Progress and future developments in modelling the climate system with general circulation models. P R Rowntree
DCTN 68	Aug 1988	A scheme for predicting layer clouds and their water content in a general circulation model. R N B Smith
DCTN 69	Nov 1988	Modelling climate change: an assessment of sea-ice and surface albedo feedbacks. W J Ingram, C A Wilson and J F B Mitchell
DCTN 70	Dec 1988	The "greenhouse" effect and climate change J F B Mitchell
DCTN 71	Dec 1988	On the dependence of climate sensitivity on convective parametrization. W M Cunnington and J F B Mitchell
DCTN 72	Dec 1988	Land surface parametrizations - basic concepts and review of schemes. P R Rowntree
DCTN 73	Jan 1989	Climate sensitivity: model dependence of results. J F B Mitchell